



Chemical, structural and electrochemical comparison of natural and synthetic FeS₂ pyrite in lithium cells

Yang Shao-Horn, Quinn C. Horn *

Energizer Inc., 25225 Detroit Road, Westlake, OH 44145, USA

Received 28 September 2000; received in revised form 26 January 2001

Abstract

Chemical composition, physical characteristics and structural features of a natural FeS₂ powder and a synthetic FeS₂ sample were correlated with their specific discharge capacities in lithium cells. The levels of impurity elements, primarily present as second-phase oxides and sulfides, were significantly higher in the natural FeS₂ than in the synthetic sample. These impure second-phases were electrochemically inactive, and they did not have any significant effects on the discharge of Li/FeS₂ cells. Trace amounts of impurity elements were detected in solid solution of FeS₂ pyrite and the pyrite structure was nearly ideal for both the natural and synthetic samples. A sulfur-deficient pyrrhotite FeS_{1.3} phase was found in the center of some large synthetic FeS₂ particles, which was electrochemically active at 1.5 V versus lithium. Optical microscopy showed that the grain sizes within synthetic FeS₂ particles were significantly smaller than those within natural FeS₂ particles. The superior rate capability of Li/synthetic FeS₂ cells was attributed primarily to the smaller grain sizes within synthetic FeS₂ particles in comparison to the natural FeS₂ sample. © 2001 Elsevier Science Ltd. All rights reserved.

Keywords: Pyrite; Lithium batteries; X-ray diffraction; Sulfide; Electron microscopy

1. Introduction

Iron pyrite FeS₂ [1] is used in commercial Energizer AA-size Li/FeS₂ primary cells at ambient temperature [2,3]. At low current densities or relatively high temperatures, Li/FeS₂ cells discharge in two steps at 1.7 and 1.5 V versus lithium, whereas under high current densities, only the 1.5 V voltage step is present [2,3]. Li/FeS₂ AA cells offer significantly longer runtime than equivalent-sized Zn/MnO₂ alkaline cells for high current density applications, particularly for current drains greater than 1 A for AA cells. At present, FeS₂ is also being

investigated as a promising positive electrode material in lithium polymer batteries for electric vehicle applications by Peled's research group [4–6]. The selection of FeS₂ pyrite samples, e.g. natural versus synthetic, which often differs in the chemical composition and physical property, affects the electrochemical performance of Li/FeS₂ cells. Natural FeS₂ powder samples normally contain notable impurities either in solid solution of pyrite or as second-phases while synthetic FeS₂ samples have high chemical and phase purity. In addition, FeS₂ samples from various sources have significantly different particle sizes and grain sizes within particles. Iwakura et al. have suggested that the superior rate capability of Li/synthetic FeS₂ cells results from the reduced particle sizes in comparison to natural FeS₂ [7,8]. Furthermore, the effect of impurity phases in the natural samples or the grain structure within FeS₂

* Corresponding author. Tel.: +1-440-8996090; fax: +1-440-8357772.

E-mail address: quinn.c.horn@energizer.com (Q.C. Horn).

Table 1

Bulk iron and sulfur compositions of the natural and synthetic FeS₂ samples determined from ICP-AES analysis and the LECO method

Major elements	Natural FeS ₂	Synthetic FeS ₂	Theoretical FeS ₂
S (wt%)	49.7	51.7	53.5
Fe (wt%)	44.2	47.6	46.5
<i>x</i> in FeS _{<i>x</i>}	2.0	1.9	2.0

particles on the performance of Li/FeS₂ cells was not studied by these authors [7,8].

X-ray diffraction, infrared, X-ray absorption and Mössbauer spectroscopy techniques have been used in studying the discharge products from Li/FeS₂ cells, however, the compositions and the structures of these reacted phases are still being poorly defined [9–16]. Several mechanisms of lithium reactions in FeS₂ pyrite have been proposed [2,7,9,10,13,16], which has been reviewed recently by Peled et al. [4]. It is generally accepted that lithium and FeS₂ react in two steps: (1) lithium ions inserting into FeS₂ to form an intermediate product, Li_{*x*}FeS₂, at 1.7 V versus lithium; (2) lithium further reacting with Li_{*x*}FeS₂ to form Li₂S and metallic Fe at 1.5 V versus lithium. It has been shown that the first reaction step is sensitive to the operating temperature and current density [2,13]. At relatively high current densities and ambient temperature, the first reaction step is suppressed and only 1.5 V voltage plateau is present, as explained by the accumulation of lithium on the surface of the particles [13]. Therefore, the first step, or the formation of Li_{*x*}FeS₂, is thought to be kinetically limiting during discharge of Li/FeS₂ cells. Chemical compositions and/or physical properties of commercial FeS₂ samples could affect the kinetics of the first step and thus the rate capability of Li/FeS₂

Table 2

Bulk impurity elements (in wt%) found in the natural and synthetic FeS₂ samples determined from ICP-AES analysis and the LECO method

Impurity elements	Natural FeS ₂	Synthetic FeS ₂
O	4.0	0.7
Si	1.7	–
Mn	0.4	–
Al	0.1	–
Ca	0.1	–
Cu	0.1	0.02
Zn	0.09	–
As	0.05	–
Co	0.02	0.02
Cr	0.004	0.01

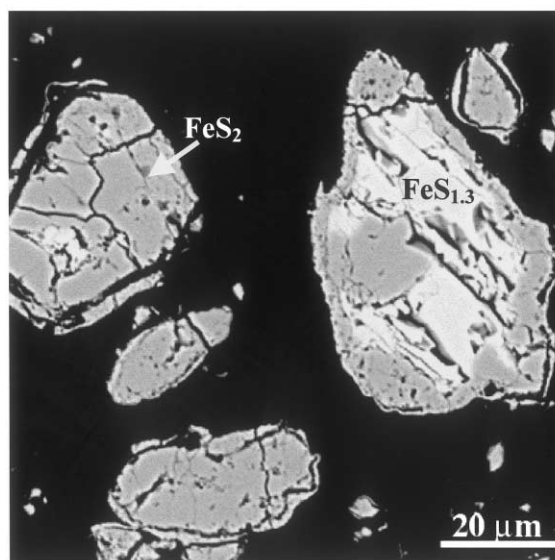
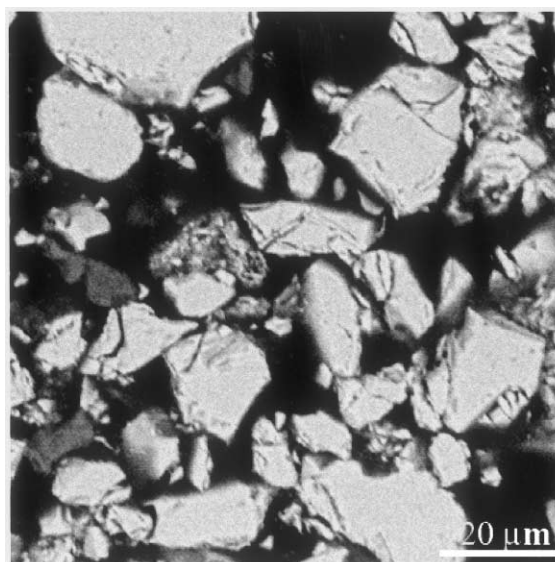


Fig. 1. BSE images of: (a) the natural; and (b) synthetic FeS₂ compressed pellets.

cells. However, correlation between FeS₂ sample characteristics and the cell performance has not been established. In order to improve the performance of Li/FeS₂ cells for high power devices, essential parameters controlling the rate capability need to be identified. In this study, we focus on determining the effects of impurity and physical properties, specifically pyrite structural parameters, particle sizes and grain sizes, on the rate capability of Li/FeS₂ cells. Chemical compositions and structural features of a commercial natural FeS₂ powder and a high-purity, synthetic FeS₂ sample were compared and then correlated with their specific discharge capacities in lithium cells. Special emphasis was

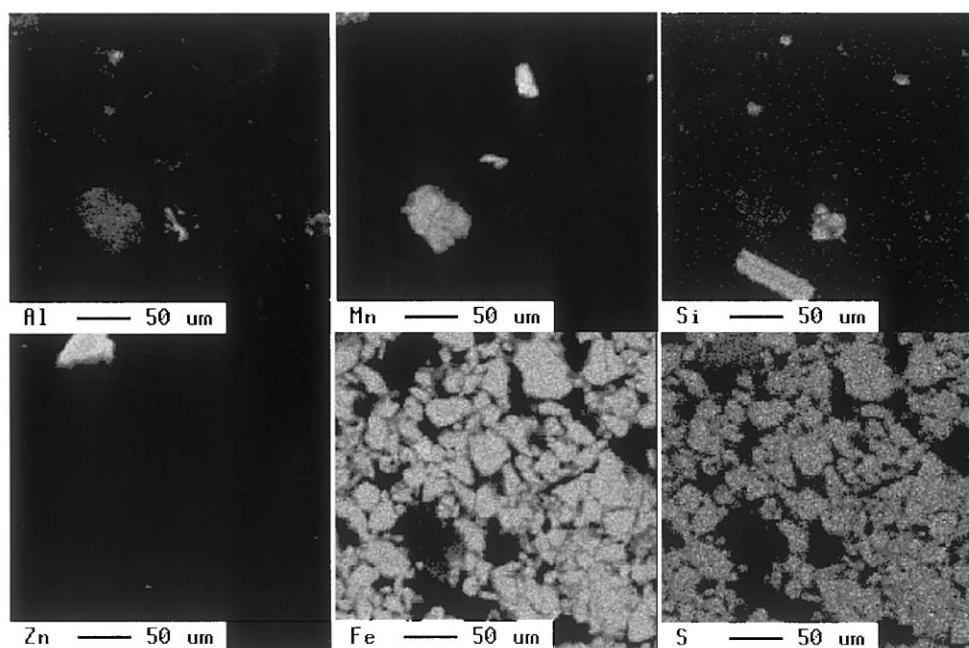


Fig. 2. Al, Mn, Si, Zn, Fe and S X-ray mapping of a natural FeS_2 pressed pellet containing 5 wt% of graphite.

placed on determining the concentrations of impurity elements in solid solution of FeS_2 pyrite structure in both natural and synthetic FeS_2 samples. Particle sizes and grain sizes within particles in these two samples were examined by scanning electron and optical microscopy. The difference in the structural parameters of FeS_2 pyrite in these two samples was determined by Rietveld refinements of X-ray powder diffraction patterns. The specific discharge capacities of lithium cells containing natural and synthetic FeS_2 electrodes were evaluated at current densities ranging from 0.3 to 300 mA g^{-1} of active FeS_2 . The findings on the impurity levels and physical parameters of the natural and synthetic FeS_2 samples were then correlated to the rate capability of lithium cells.

2. Experimental

Bulk chemical compositions of a natural FeS_2 pyrite (Chemetall) and an Alpha AESAR synthetic FeS_2 (99.9% purity, metals basis) samples were determined by inductively coupled plasma-atomic emission spectroscopy (ICP-AES) and the LECO method (ASTM D4239-83). In order to examine whether iron and sulfur was distributed uniformly, backscattered electron (BSE) imaging was performed on metallographically polished surfaces of compressed FeS_2 pellets containing 5 wt% graphite. In order to determine the impurities in solid solution of FeS_2 pyrite, electron probe microanalysis

(EPMA) of the FeS_2 pellets was used on a JEOL 8400 Superprobe equipped with wavelength dispersive spectrometers. Quantitative element analysis was conducted using JEOL correction software and ZAF correction algorithms. The EPMA was standardized for the elements using certified elemental or mineral standards for each of the elements. The following analysis conditions were used for the microprobe: an accelerating voltage of 20 kV, a probe current of 5.0×10^{-8} A, focused beam, and counting times of 60 s for both peak and background.

Table 3

The average concentrations of iron, sulfur and impurity elements present in Fe-S containing particles in the natural and synthetic samples determined from EPMA

Elements	Natural FeS_2	Synthetic FeS_2
Fe (at%)	33.11 ± 0.43	33.31 ± 0.33 43.66 ± 0.47
S (at%)	66.65 ± 0.45	66.22 ± 0.34 55.74 ± 0.62
x in FeS_x	2.0	2.0 1.3
Cu (wt%)	0.01–0.71 (avg. 0.1)	None–0.023 (avg. 0.01)
As (wt%)	None–0.2 (avg. 0.05)	None
Co (wt%)	None–0.1 (avg. 0.015)	None
Si (wt%)	0.011–0.034 (avg. 0.018)	None

Table 4

Weight fractions of Fe–S containing phases in the natural and synthetic FeS₂ samples summarized from chemical analysis results

Weight fractions of Fe–S containing phases	Natural FeS ₂	Synthetic FeS ₂
FeS ₂ pyrite (wt%)	95	89
FeS _{1.3} (wt%)	–	11
Calculated specific capacity (mA h g ⁻¹)	850	870

Particle size distributions were analyzed using a Microtrac X100. The particle sizes and morphologies were also examined using scanning electron microscopy (LEO 438VP). Grain microstructures within particles were developed from etching metallographically prepared, epoxy mounted FeS₂ samples using 50% nitric acid, and then were recorded by optical microscopy (Olympus Vanox Optical Microscope). Primary and secondary phases, and structural parameters of the natural and synthetic FeS₂ samples were determined by X-ray diffraction analysis with CuK_α radiation on a Siemens D5000 diffractometer equipped with a graphite monochromator. Structural parameters of the pyrite structure in the two samples were refined from the X-ray powder diffraction data using the Rietveld method (GSAS software). The X-ray diffraction patterns

used for structural refinements were collected in the 2θ range of 10–120°, at a step size of 0.02° and a step time of 15 s.

Specific discharge capacities of the natural and synthetic FeS₂ electrodes were evaluated in 2016 lithium coin cells under galvanostatic conditions. An 11-mil thick lithium foil was used as the anode in the cell. The electrode formulation consisted of 92.75 wt% FeS₂, 4.75 wt% carbon, 2.50 wt% binder. Electrode mix slurry was made using trichloroethylene as the solvent. Thin pellet-type electrodes compressed into expanded aluminum meshes at 5000 psi were produced from a dried mix that was obtained by evaporating the solvent off the electrode mix slurry. The active weight per electrode was 50 mg and the electrode area was 1.88 cm². This corresponds to a loading density of 26 mg cm⁻². Two pieces of Celgard 2500 separator were used in all of the coin cells. The electrolyte was prepared by dissolving 1 M LiCF₃SO₃ in 24.95 vol% Dioxolane, 74.85 vol% Dimethoxyethane and 0.2 vol% Dimethylisoxazole. Galvanostatic tests of 2016 Li/FeS₂ coin cells was performed at current densities of 0.3, 1.5, 3, 10, 30, 100, 213 and 300 mA g⁻¹ of active FeS₂, respectively, on an Arbin test system at 21 ± 2°C. Three coin cells were assembled and tested per current density selected. In general, the experimental variation in the specific capacities of three equivalent cells falls within ± 25 mA h g⁻¹ of the average value. Therefore, the average specific capacity was used for comparison between the natural and synthetic FeS₂ under each current density condition.

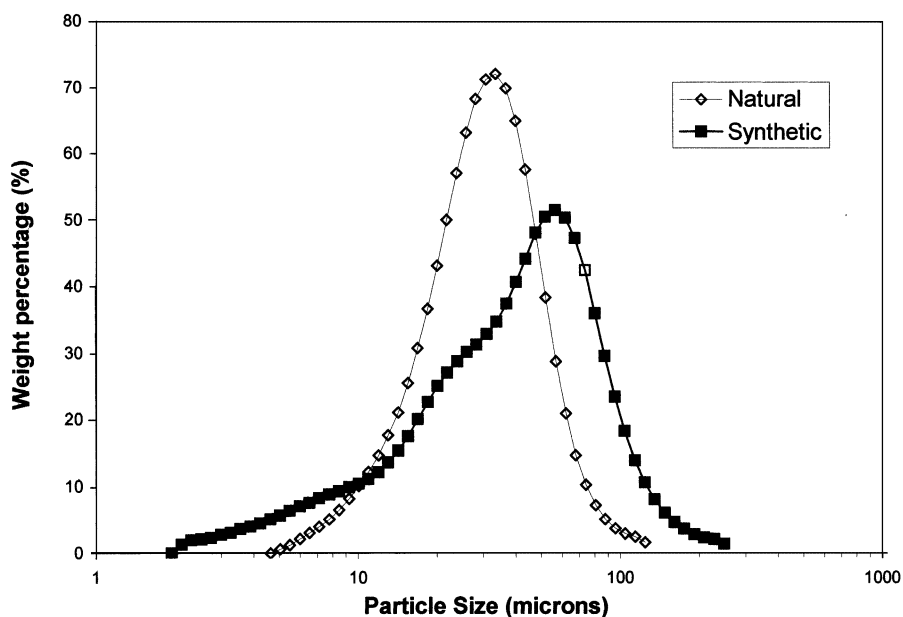


Fig. 3. Particle size distributions of the natural and synthetic FeS₂ samples measured by Microtrac.

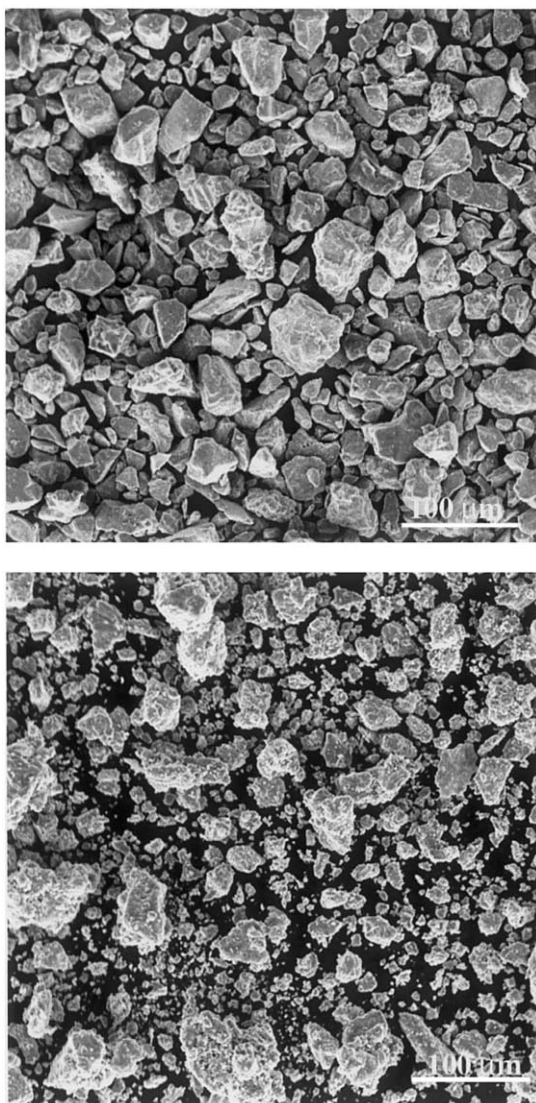


Fig. 4. SEM images of: (a) natural; and (b) synthetic FeS_2 samples at $500\times$, which shows the typical particle sizes and morphologies of these two samples.

3. Results and discussion

3.1. Chemical composition

Bulk iron and sulfur contents of the natural and synthetic FeS_2 pyrite samples are shown in Table 1. It should be noted that the S/Fe atomic ratio in the natural sample was consistent with the theoretical value, but higher than that in the synthetic sample. Bulk impurity elements in both FeS_2 samples are listed in Table 2. As expected, natural samples had significant more impurity elements than the synthetic sample. In the natural FeS_2 sample, Si and O were the major impurity elements, most likely in the form of SiO_2 . In

addition, a large number of metal impurity elements, such as Mn, Al, Ca, Cu, Zn, As and Co, were detected. If all of the iron detected in the natural sample were present in the FeS_2 pyrite phase, the weight percentage of FeS_2 pyrite would be 95%, which corresponded to a theoretical specific capacity of 850 mA h g^{-1} in lithium cells. In contrast, in the synthetic sample, oxygen and metal impurity contents were significantly lower than those of the natural sample. If all of the sulfur detected in the synthetic sample were present in the FeS_2 pyrite, the weight percentage of FeS_2 pyrite would be 97%, which suggested a theoretical specific capacity of 870 mA h g^{-1} . Therefore, the natural and synthetic FeS_2

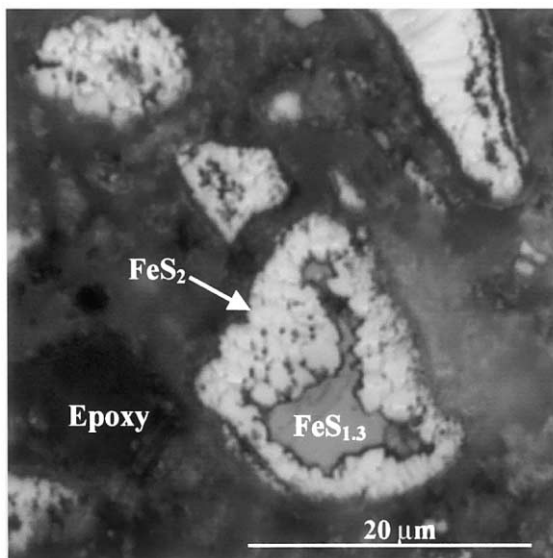
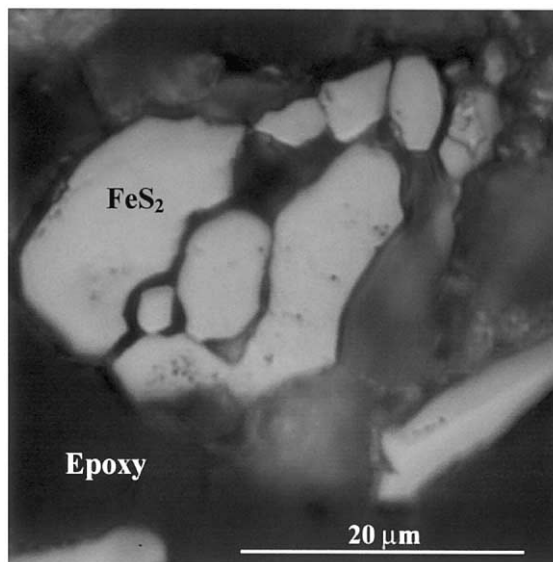


Fig. 5. Optical images of grains structures within the: (a) natural; and (b) synthetic FeS_2 particles.

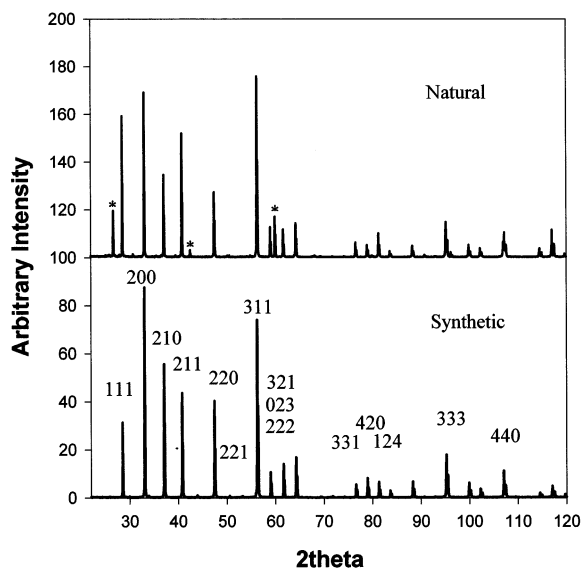


Fig. 6. X-ray powder diffraction patterns of the natural and synthetic FeS_2 samples with CuK_α radiation.

electrodes had comparable theoretical specific capacities in lithium cells.

The elements revealed from bulk chemical analysis, particularly the impurity elements, might not distribute uniformly within the FeS_2 samples. In order to examine whether iron and sulfur was distributed uniformly within one particle, backscattered electron (BSE) imaging was performed on metallographically polished surfaces of compressed natural and synthetic FeS_2 pellets containing 5 wt% graphite. Uniform brightness in the BSE images (Fig. 1a) was observed for all of the iron–sulfur (Fe–S) containing particles in the natural sample, which corresponded to a uniform composition within each particle. BSE imaging of the synthetic sample, however, showed non-uniform brightness of some large synthetic FeS_2 particles that were approximately greater than 20 μm . As shown in Fig. 1b, the regions near the center of the large particles appeared brighter in the BSE image and had a higher average atomic number than the surrounding region. The volume fraction of the bright, center regions in the BSE images was 11%, which was obtained from the area

Table 5

The lattice parameter and sulfur position parameter of the pyrite structure in the natural and synthetic FeS_2 samples

Structural parameters	Natural FeS_2	Synthetic FeS_2
Lattice parameter	0.5419(1)	0.54182(3)
Sulfur positional parameter x	0.385(2)	0.385(1)

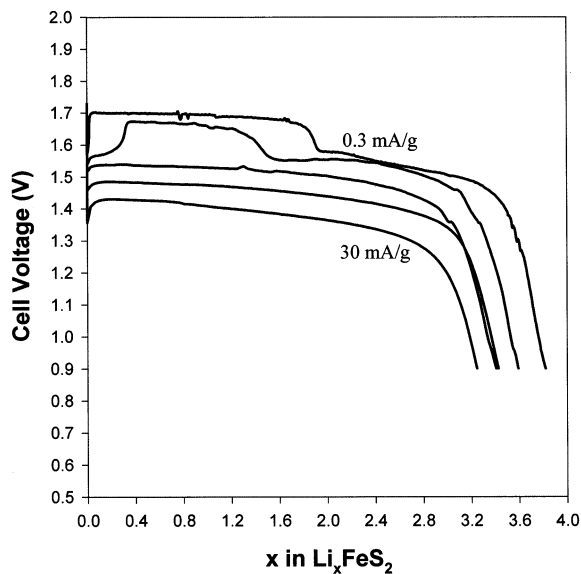


Fig. 7. Typical discharge profiles of natural FeS_2 cells at current densities of 0.3, 1.5, 3, 10 and 30 mA g^{-1} , with a cell voltage cutoff of 0.9 V.

fraction determined from image analysis of 35 areas with a magnification of 1000 \times . The exact compositions of these Fe–S containing particles in the natural and synthetic FeS_2 samples will be further determined by EPMA. X-ray element mapping in the scanning electron microscope was used to locate the impurity elements in the FeS_2 samples. As shown in Fig. 2, the

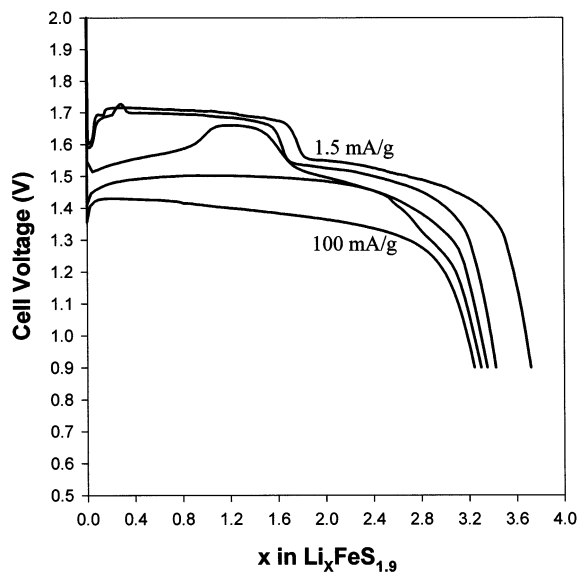


Fig. 8. Typical discharge profiles of synthetic FeS_2 cells at current densities of 1.5, 3, 10, 30 and 100 mA g^{-1} , with a cell voltage cutoff of 0.9 V.

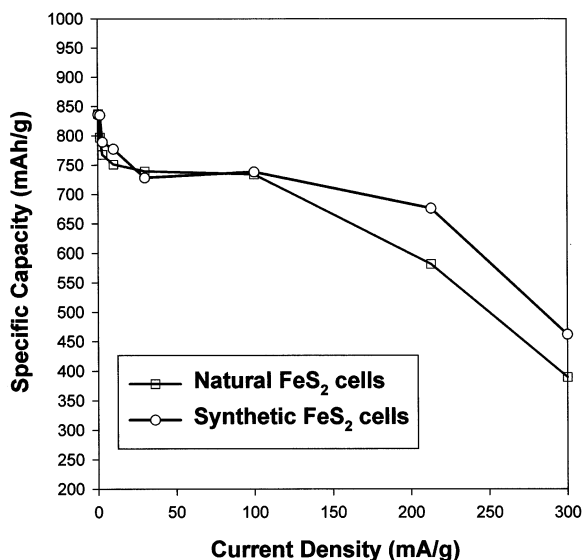


Fig. 9. Average specific capacities of natural and synthetic FeS₂ cells as a function of current density.

impurity elements in the natural sample were mostly present in second-phase oxides, such as aluminum manganese oxides and silicon oxides. They are most likely electrochemically inactive in Li/FeS₂ cells. X-ray mapping of the synthetic sample did not reveal any non-Fe–S containing particles.

In order to quantify the iron and sulfur contents, and impurity levels of Fe–S containing particles in the natural and synthetic samples, polished, compressed natural and synthetic FeS₂ pellets were further determined by EPMA. The average concentrations of iron, sulfur and the impurities in both samples are shown in Table 3. Analysis of more than 50 particles in the natural sample revealed that all of them had the stoichiometric FeS₂ composition within experimental uncertainty. As expected from the BSE results, EPMA analysis of Fe–S containing particles in the synthetic sample revealed two distinct compositions, stoichiometric FeS₂ and FeS_{1.3}, which corresponded to the gray and white regions in Fig. 1b, respectively. Trace levels of Cu, As, Co and Si were found in solid solution of natural FeS₂. Note that the concentrations of the impurity elements were found to vary considerably among different natural FeS₂ particles. In contrast to the natural FeS₂, only Cu impurity was detected in the Fe–S containing particles in the synthetic sample. Such minute levels of impurity elements in solid solution in the natural and synthetic samples are unlikely to have any significant effects on the structural parameters of FeS₂ pyrite or the rate capability of Li/FeS₂ cells.

Observation of sulfur-deficient component, FeS_{1.3}, in the center of large FeS₂ particles is significant as it

affects the specific discharge capacities and/or the rate capability of Li/FeS₂ cells. Sulfur deficiency in synthesizing FeS₂ is expected from the Fe–S phase diagram. The FeS₂ phase is adjacent to the Fe_{1–y}S (or FeS_x) + FeS₂ + S (vapor) and the FeS₂ + liquid S + S (vapor) phase fields between 743 and 400°C [17,18]. The formation of FeS₂ layers on the surfaces of Fe_{1–y}S particles would inhibit any further reactions between Fe_{1–y}S in the center and sulfur vapor surrounding the particles. The presence of FeS_{1.3} in the synthetic sample was later confirmed by X-ray diffraction analysis. If FeS_{1.3} had a density similar to FeS₂ pyrite, the weight fraction of FeS_{1.3}, calculated from the bulk chemical composition of the synthetic sample, would be consistent with the volume fraction of this phase determined from the BSE area measurements.

In summary, among the Fe–S containing particles, only FeS₂ was found in the natural sample while both FeS₂ and FeS_{1.3} were revealed in the synthetic sample, as listed in Table 4. As they are the electrochemically active phases in lithium cells, at low current densities, similar discharge capacities are expected for the natural and synthetic FeS₂ electrodes.

3.2. Physical characterization

The particle size distribution of the natural FeS₂ sample was much tighter than that of synthetic sample, as shown in Fig. 3. A mean particle size of 30 μm was found for the natural sample while the synthetic sample appeared to have a mixture of two particle size distributions with means of 20 and 60 μm. In addition, scanning electron microscopy clearly revealed the difference in the particle sizes and morphologies of these two samples in Fig. 4a and b. A significant amount of relatively small FeS₂ particles was found in the synthetic sample in comparison to the natural FeS₂. Furthermore, the grain structures within FeS₂ particles of the natural and synthetic samples are shown in Fig. 5a and b, respectively. Each natural FeS₂ particle comprised of a few relatively large grains whereas each synthetic particle contained many small FeS₂ grains on the exterior of the particle and the FeS_{1.3} component in the center of the particles. It should be noted that the grain sizes (5–15 μm) within natural FeS₂ particles (Fig. 5a) were much larger than those (0.5–2 μm) within synthetic FeS₂ particles (Fig. 5b). The grain structure of FeS_{1.3} in the center of the synthetic particles was not resolved by etching, as shown in Fig. 5b. It is believed that small grain sizes of FeS₂ enhance the kinetics of lithium inserting into in FeS₂ to form Li_xFeS₂. Therefore, the synthetic FeS₂ electrodes were expected to have superior rate capability to the natural FeS₂ electrodes in lithium cells.

3.3. Structural characterization

X-ray powder diffraction patterns of the as-received natural and synthetic FeS₂ samples are shown in Fig. 6. The natural sample had SiO₂ quartz as the primary impurity phase (marked by stars). In contrast, the synthetic FeS₂ sample appeared to be phase pure, indexed to the FeS₂ pyrite structure in Fig. 6 [1]. The X-ray diffraction peak intensities of the FeS_{1.3} component are barely visible. As similar chemical compositions were found in the natural FeS₂ particles and the FeS₂ component of the synthetic sample, no significant difference in the structural parameters was expected. The lattice parameter of the pyrite structure and the sulfur position parameter in the natural and synthetic samples were determined by the Rietveld refinements of X-ray powder diffraction data. The refinement results showed that the pyrite structure was nearly ideal in both the natural and synthetic FeS₂ samples, as listed in Table 5. This confirmed that trace levels of impurity elements in solid solution did not have any significant effects on the FeS₂ pyrite structure.

It should be noted that the relative peak intensities of these two samples are considerably different. The difference in relative peak intensities was eliminated by grinding the natural FeS₂ powder in a mortar–pestle prior to X-ray analysis, which suggested that this difference be related to the orientation effect of large natural FeS₂ particles. The grinding process also resulted in increased peak intensities of the FeS_{1.3} (or Fe_{1-y}S, $y=0.2$) component in the synthetic sample, which could be matched to hexagonal pyrrhotite Fe_{1-y}S [19]. It should be pointed out that the hexagonal pyrrhotite phase in the synthetic sample is metastable at ambient temperature, as it has the minimum stability temperature of 100°C [18]. As pyrrhotite FeS_{1.3} has a density of 4.98 g cm⁻³ [19], nearly identical to that of FeS₂ pyrite (5.01 g cm⁻³) [1], the weight fraction is comparable to the volume fraction of pyrrhotite FeS_{1.3} in the synthetic sample. It is confirmed that the weight fraction of this phase deduced from chemical analysis (Table 4) was consistent with the volume fraction determined from BSE area measurements.

In short, chemical, physical and structural characterization showed that the most noticeable differences between the natural and synthetic FeS₂ particles were the grain sizes, the particle size distributions and the presence of sulfur-deficient pyrrhotite FeS_{1.3} phase. At low current densities, similar specific discharge capacities are expected for natural and synthetic FeS₂ electrodes (Table 4). Lithium cells containing synthetic FeS₂ electrodes, with much smaller FeS₂ grains and significantly more small FeS₂ particles are expected to have superior rate capability to those with natural FeS₂ electrodes.

3.4. Electrochemical characterization

Galvanostatic test results of 2016 lithium cells containing the natural and synthetic FeS₂ electrodes tested at a range of current densities are compared in Figs. 7 and 8, respectively. The lithium content in the fully discharged natural FeS₂ electrodes, or x in Li _{x} FeS₂, was adjusted for a sample purity of 95 wt%. As expected, similar voltage profiles and lithium contents (or specific discharge capacities) were found for the natural and synthetic FeS₂ cells. This result confirmed that the impure second-phases in the natural FeS₂ sample were electrochemically inactive, and they did not have any significant effects on the discharge of Li/FeS₂ cells. Careful examination of voltage profiles in Figs. 7 and 8 suggested that lithium reactions in FeS_{1.3} occurred at 1.5 V versus lithium, which was consistent with the previous work on FeS_{1.1} [20]. A two-step reaction at 1.7 and 1.5 V gradually transformed to a one-step reaction at 1.5 V as current densities increased, consistent with the previous studies [2,13]. However, it should be noted that the transition from the two-step to the one-step occurred at significantly higher current densities for synthetic FeS₂ cells than for natural FeS₂ cells. Moreover, at current densities higher than 100 mA g⁻¹, the average specific capacities of synthetic FeS₂ cells were significantly higher than natural FeS₂ cells, as shown in Fig. 9. These results showed that the synthetic FeS₂ electrodes had better rate capability than the natural FeS₂ in lithium cells. It is believed that the superior rate capability of synthetic FeS₂ cells was attributed primarily to the smaller grain sizes within synthetic FeS₂ particles in comparison to the natural FeS₂ sample.

4. Conclusions

The most noticeable differences between the natural and synthetic FeS₂ particles were the grain sizes, the particle size distributions and the presence of sulfur-deficient pyrrhotite FeS_{1.3} phase. Impure second-phases in the natural FeS₂ sample were electrochemically inactive, and they did not have any significant effects on the discharge of Li/FeS₂ cells. Trace impurity elements in solid solution of FeS₂ pyrite and the ideal pyrite structure were found for both natural and synthetic FeS₂ samples. The superior rate capability of synthetic FeS₂ cells was attributed primarily to the smaller grain sizes within synthetic FeS₂ particles in comparison to the natural FeS₂ sample.

Acknowledgements

Dr Andrew Webber, Dr Richard Middaugh and Mr Jack Marple are acknowledged for fruitful discussions

and reviewing this report. The author would like to thank Steve Osmialowski, and Ruth Sholtis-Furyes for laboratory assistance and microscopy studies.

References

- [1] Joint Commission of Powder Diffraction File Sets, File # 42-1340, International Center for Diffraction Data, Newtown Square, PA.
- [2] M.B. Clark, Lithium–Iron Disulfide Cells, in: J.-P. Gabano (Ed.), *Lithium Batteries*, Academic Press, New York, 1982.
- [3] J.C. Nardi, M.B. Clark, W.P. Evans, Symposium on Electric Power Sources in Horological and Micro-technical Products, Mulhouse, France, Extended Abstract, 48, April 1981.
- [4] D. Golodnitsky, E. Peled, *Electrochim. Acta* 45 (1999) 335.
- [5] S. Kostov, M. denBoer, E. Strauss, D. Golodnitsky, S.G. Greenbaum, E. Peled, *J. Power Sources* 81/82 (1999) 709.
- [6] E. Strauss, G. Ardel, V. Livshits, L. Burstein, D. Golodnitsky, E. Peled, *J. Power Sources* 88 (2000) 206.
- [7] H. Ikeda, S. Narukawa, S. So, H. Tamura, C. Iwakura, Proc. 30th Power Sources Symp., 1982, p. 179.
- [8] C. Iwakura, N. Isobe, H. Tamura, *Electrochim. Acta* 28 (1983) 269.
- [9] Z. Tomczuk, B. Tani, N.C. Otto, M.F. Roche, D.R. Vissers, *J. Electrochem. Soc.* 129 (1982) 925.
- [10] C. Iwakura, N. Isobe, H. Tamura, *Electrochim. Acta* 28 (1983) 277.
- [11] P. Gard, C. Sourisseau, G. Ouvrard, R. Brec, *Solid State Ionics* 20 (1986) 231.
- [12] D. Bernardi, J. Newman, *J. Electrochem. Soc.* 134 (1987) 1309.
- [13] R. Fong, J.R. Dahn, C.H.W. Jones, *J. Electrochem. Soc.* 136 (1989) 3206.
- [14] C.H.W. Jones, P.E. Kovacs, R.D. Sharma, R.S. McMillan, *J. Phys. Chem.* 94 (1990) 832.
- [15] C.H.W. Jones, P.E. Kovacs, R.D. Sharma, R.S. McMillan, *J. Phys. Chem.* 95 (1991) 774.
- [16] D. Tryk, S. Skim, Y. Hu, W. Xing, D. Scherson, M. Antonio, V. Leger, G. Blomgren, *J. Phys. Chem.* 99 (1995) 3732.
- [17] E.A. Brandes, G.B. Brook (Eds.), *Smithells Metals Reference Book*, 7th ed., Linacre House, Jordan Hill, Oxford, Butterworth–Heinemann, London, 1992, pp. 11–269.
- [18] J.R. Craig, S.D. Scott, *Sulfide Phase Equilibria, Sulfide Mineralogy*, vol. 1, Mineralogical Society of America, 1974 (p. CS21).
- [19] Joint Commission of Powder Diffraction File Sets # 22-1120.
- [20] Y. Uetani, K. Yokoyama, O. Okamoto, *J. Power Sources* 5 (1980) 89.